Sensing and Bio-Sensing Research 5 (2015) 62–70

Contents lists available at ScienceDirect

Sensing and Bio-Sensing Research

journal homepage: www.elsevier.com/locate/sbsr

A novel deflection shape function for rectangular capacitive micromachined ultrasonic transducer diaphragms

Zhou Zheng [a], Weijie Sun [a], Xudong Suo [a], Lawrence L.P. Wong [b], Zhendong Sun [c], John T.W. Yeow [b,*]

[a] Department of Automation Science and Engineering, South China University of Technology, Guangzhou 510641, China
[b] Department of Systems Design Engineering, University of Waterloo, Waterloo, ON N2L 3G1, Canada
[c] Academy of Mathematics & Systems Science, Chinese Academy of Science, Beijing 100190, China

ARTICLE INFO

Article history:
Received 16 May 2015
Revised 11 July 2015
Accepted 14 July 2015

Keywords:
Capacitive micromachined ultrasonic transducers
Finite element analysis
Deflection shape function

ABSTRACT

A highly accurate analytical deflection shape function that describes the deflection profiles of capacitive micromachined ultrasonic transducers (CMUTs) with rectangular membranes under electrostatic pressure has been formulated. The rectangular diaphragms have a thickness range of 0.6–1.5 μm and a side length range of 100–1000 μm. The new deflection shape function generates deflection profiles that are in excellent agreement with finite element analysis (FEA) results for a wide range of geometry dimensions and loading conditions. The deflection shape function is used to analyze membrane deformations and to calculate the capacitances between the deformed membranes and the fixed back plates. In 50 groups of random tests, compared with FEA results, the calculated capacitance values have a maximum deviation of 1.486% for rectangular membranes. The new analytical deflection function can provide designers with a simple way of gaining insight into the effects of designed parameters for CMUTs and other MEMS-based capacitive type sensors.

1. Introduction

Capacitive micromachined ultrasonic transducers (CMUTs) have been making significant impact in many fields such as medical diagnostic ultrasound, structural health detecting and real-time monitoring of machinery operation [1,2]. CMUT-based sensors are ideal for these purposes due to their high sensitivity, small size, low mass, long lifetime and low power requirement. A CMUT with a rectangular diaphragm is shown in Fig. 1. It consists of a dielectric spacer-supported clamped rectangular diaphragm and a fixed back plate, which are separated by a thin gap. When an external pressure is exerted onto the sensor, the top membrane will deform, leading to a dynamic change in the capacitance between the deformed membrane and the fixed back plate [3].

Highly accurate analytical deflection shape functions that describe the deflection of deformed CMUT membranes will not only provide the insight into the CMUT design methodology but also ascertain the effect of specific geometry parameters [4–11]. For these reasons, deflection shape functions of square and circular membranes have been widely studied by many authors.

Plate theory is often applied to capture the functional form of the deformation curve. The transverse deflection $\omega(x, y)$ of any point (x, y) on a uniformly loaded diaphragm can be obtained by energy minimization method [12]. However, this method is computationally intensive as solutions of numerous simultaneous nonlinear equations are required. Some simple analytical deflection models, the accuracy of which depends mainly on the deformed membrane shape, have been used to predict the deformed curves of square membranes. The deflection model of a rigidly clamped square membrane under a uniform external pressure was first presented as a cosine-like function as [12]

$$\omega(x,\ y) = \omega_0 \cdot \cos\frac{\pi x}{2a} \cdot \cos\frac{\pi y}{2a}, \tag{1}$$

where a is half the side length of the diaphragm and ω_0 is the center deflection. This function describes the general membrane deflection shape, but not accurately. In order to achieved desirable accuracy, authors in [13] expanded the function with two more terms to yield

$$\omega(x,\ y) = \omega_0\left[1 + 0.4 \cdot \frac{x^2+y^2}{a^2} + 1.16 \cdot \frac{x^2y^2}{a^4}\right] \cdot \cos\frac{\pi x}{2a} \cdot \cos\frac{\pi y}{2a}. \tag{2}$$

However, authors in [14] pointed out that function (2) fails to catch the deflection profiles of thick membranes, although it agree well with those of thin and large ones. And a new deflection model was introduced in [14] to cover different cases by squaring the cosine terms and adding a new term.

* Corresponding author.
E-mail address: jyeow@uwaterloo.ca (J.T.W. Yeow).

http://dx.doi.org/10.1016/j.sbsr.2015.07.006
2214-1804/

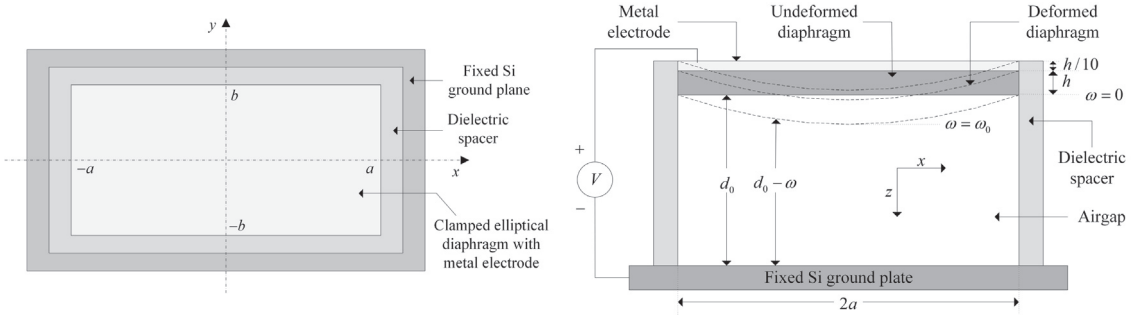

(a) Top view. (b) Cross sectional view [15].

Fig. 1. Top and cross-sectional view of a conceptual CMUT device with rectangular diaphragm.

Authors in [15] further improved the accuracy by developing a new deflection model for square membranes following a two-step process. In the process, the center deflection ω_0 is first obtained by solving a load–deflection model, then the deformed diaphragm shape $\omega'(x, y)$, which is independent from the center deflection, is calculated and multiplied by ω_0 to obtain the complete deflection profile. The load–deflection model of a square diaphragm under a uniform pressure P_M can be expressed as [15]

$$P_M = \left[C_r \frac{\sigma_0 h}{a^2} + C_b \frac{12D}{a^4}\right]\omega_0 + \left[C_s f_s(v) \frac{Eh}{a^4(1-v^2)}\right]\omega_0^3 \quad (3)$$

where σ_0 is residual stress, h is membrane thickness, v is Poisson's ratio. The Poisson's ratio dependent function $f_s(v)$ is given as $f_s(v) = \frac{1-0.271v}{1-v}$. D is the flexural rigidity of the membrane expressed as $D = \frac{Eh^3}{12(1-v^2)^2}$, where E is the Young's modulus of the diaphragm material. The constants C_r, C_b and C_s are determined by comparing the deflection profiles in (3) with finite element analysis (FEA) results [16].

Following the two-step process, the analytical deflection model for CMUT with square membrane was presented as [15]

$$\omega(x, y) = \omega_0\left(1 - \frac{x^2}{a^2}\right)^2\left(1 - \frac{y^2}{a^2}\right)^2 \sum_{n=0,1,2}^{N} c_n\left(\frac{x^2+y^2}{a^2}\right)^n. \quad (4)$$

The polynomial basis function was substituted for cosine basis function and higher accuracy was obtained. Function (4) was subsequently used to calculate the capacitance values of CMUTs by formula as

$$C_{Deform} = \varepsilon_0 \iint_A \frac{dxdy}{d_0 - \omega(x, y)}, \quad (5)$$

where d_0 is the gap thickness, and ε_0 is the permittivity of free space, given as $\varepsilon_0 = 8.85 \times 10^{-12}$ F/m.

It has been shown that FEA provides highly accurate deflection profiles for CMUT membranes and other MEMS-based transducers [17–21]. But it does not give an insight into the influences of the device geometries on CMUTs as analytical models do. The capacitance calculated by the analytical deflection models (2) and (4) has a good agreement with the FEA results for square diaphragms [15]. However, deflection shape function of rectangular membranes has never been studied, probably due to their complexities in deflection shape. In fact, rectangular membranes are worth studying because they have shown the potential in improving the fill factor and the performance of CMUTs compared with square ones [22,23].

As mentioned above, the accuracy of the analytical deflection model depends not only on the diaphragm's center deflection ω_0, but also on the shape of the deformed membrane $\omega'(x, y)$. This paper focuses on the determination of the deformed diaphragm shapes. We will study a much more general case of membranes and formulate highly accurate deflection shape functions for CMUTs with rigidly clamped rectangular membranes. A data fitting technique is applied to identify the parameters in the deflection shape function by using MATLAB. The effectiveness of the deflection shape function will be illustrated by comparing the predicted deflection profiles with FEA results (using *ANSYS 15.0 software, ANSYS Inc.*). For various clamped CMUT membranes with different geometry dimensions and loading conditions, the new deflection shape function shows excellent agreement with corresponding FEA results.

2. Finite element analysis of CMUT

The 3D FEA model is chosen to simulate the deformation of the membrane. In the finite element simulation, a DC bias voltage (expressed as U) is applied between the electrodes to exert an electrostatic force on the diaphragm. As the bias voltage increases from zero across the membrane and the fixed back plate, the distance between them would decrease until the two plates suddenly snap into contact. This behavior is called the pull-in effect, and the transition voltage is called pull-in voltage. The loading condition on the diaphragm which causes pull-in effect is neglected in the simulation. The device specifications in our simulations are listed in Table 1.

The membrane is modeled by SOLID 186 element while TRANS 126 is employed to apply the electrostatic force on the diaphragm. Considering the symmetrical characteristic of the diaphragm, we use only 1/4 of the diaphragm in the simulation so as to improve the computational efficiency. For boundary conditions, the edges of the membrane are strictly clamped. As shown in Table 2, comparison of center deflections between our simulation results and those in [15] has been conducted to verify the effectiveness of our simulation method. Note that the top electrode is ignored at first to keep consistent with simulations in [15].

It can be observed from Table 2 that our simulation results are nearly the same as those in [15], thus demonstrating that our simplified simulation method insures the accuracy while improving the operational speed.

To simulate the practical operation of CMUTs, a top electrode is added in the finite element model. It has the same width and

Table 1
Device specifications.

Parameter (Unit)	Si_3N_4 diaphragm	Al electrode
Young's modulus (GPa)	169	67.6
Poisson ratio	0.3	0.3555
Density (kg/m^3)	2332	2700
Residual stress (MPa)	50	10

Table 2
Comparison of center deflections of square membranes between our simulation results and those in [15]. $a = 100$ μm, $d_0 = 3$ μm, $\sigma_0 = 100$ MPa, $U = 12$ V.

Deflection	h (μm)	P_M (kPa)	ω_0 (μm)	
			[15]	Our simulation
Small	1	20	0.43	0.431
	2	160	1.08	1.082
	3	400	1.18	1.181
Large	1	60	1.16	1.164
	2	480	2.50	2.506
	3	1000	2.49	2.504

length as those of the diaphragm, while its thickness is 1/10 of the membrane thickness. Uniform pressure is withdrawn in the following simulations because pressure on CMUTs are generally not uniform in practical situations.

3. New deflection shape functions

In this section, the analytical deflection model for CMUTs with rectangular diaphragms is established. The rectangular diaphragms of interest have a thickness range of 0.6–1.5 μm and a side length range of 100–1000 μm. Each edge of the rectangular diaphragm is rigidly clamped and the deflection profile is determined by inner strain in the x and y directions as well as external pressure from the z direction. In the analytical model, a is half of the long side, b is half of the short side, h is the thickness of membrane, and $n = a/b (n \geqslant 1)$ denotes the aspect ratio.

Assuming that the deflection shape function for the rectangular membranes is similar to that for the square ones in [15] and has the following form

$$\omega'(x,\ y) = \left(1 - \frac{x^2}{a^2}\right)^2 \left(1 - \frac{y^2}{b^2}\right)^2 \left(1 + c_1 \frac{x^2}{a^2} + c_2 \frac{x^4}{a^4} + c_3 \frac{y^2}{b^2} + c_4 \frac{y^4}{b^4}\right), \tag{6}$$

where the parameters c_1, c_2, c_3 and c_4 are determined by comparing the function with the FEA results. $\omega'(x, 0)$ and $\omega'(0, y)$ represent the deflection shape of the diaphragm along x-axis and y-axis, respectively.

Fig. 2 shows the deviation error from the FEA results with the aspect ratio n against the standardized coordinate of x-axis and y-axis when the membrane thickness is 1 μm. Negligible deviation error can be observed from Fig. 2(b) as n varies from 1 to 10, which reveals that function (6) can well predict the deformation profile along y-axis. However, Fig. 2(a) shows that the deviation error along x-axis is significant when the aspect ratio n is greater than four, while it is negligible when n is less than 4. Therefore, the function should be modified to improve the accuracy, especially in the cases when $n \geqslant 4$.

To achieve this goal, basic functions must be selected first. It is known that some basic functions have been used in $\omega'(x, y)$ to capture the deformed nonlinear behavior of the diaphragms [12–15]. $R_1(x)$, $R_2(x)$ and $R_3(x)$ are some of them that have been employed in previous researches in square diaphragm cases

$$R_1(x) = \left(1 - \left(\frac{x}{a}\right)^2\right)^2, \tag{7}$$

$$R_2(x) = \cos\left(\frac{\pi x}{2a}\right), \tag{8}$$

$$R_3(x) = \cos^2\left(\frac{\pi x}{2a}\right). \tag{9}$$

Investigations have been conducted to determine whether these basic functions are still available for rectangular membranes. Two membranes with different geometry dimensions are employed to represent each case ($n < 4$ and $n \geqslant 4$). Figs. 3 and 4 show comparisons of curve shapes between the basic functions and the FEA results when $n < 4$ and $n \geqslant 4$, respectively. Both figures reveal that the existing basic functions, R_1 in particular, are still able to describe the general shape of the deformed membrane along y-axis. It can be observed from Fig. 3(a) that they are also available for x-axis when $n < 4$. However, in the case of $n \geqslant 4$, as shown in Fig. 4(a), all the three function fail to capture the deformed curve along x-axis.

For further investigation, method of least squares is employed to estimate the errors between the basic functions and the FEA results. The values of S_1, S_2 and S_3, which are the summed squares of residuals between the FEA results and functions R_1, R_2 and R_3, and calculated by 21 data points, respectively, are shown in Table 3.

Apparently, the same conclusion can be drawn from Table 3 as that from the curve comparisons. Therefore, a new basic function should be found for x-axis when $n \geqslant 4$, while function R_1 could serve as the basic function for other cases.

By comparing the deformed membrane curve with an exponential function in Fig. 5, it can be observed that the curve of the new function is close to that of the FEA results. Besides, the summed square of residuals between the new function and the FEA results is calculated as 0.36 along x-axis, much less than previous estimated values. Therefore, the exponential function

$$R_4(x) = 1 - 0.2^{a-x} \tag{10}$$

is proposed as the new basic function to capture the deformed shape of the membrane along x-axis when $n \geqslant 4$.

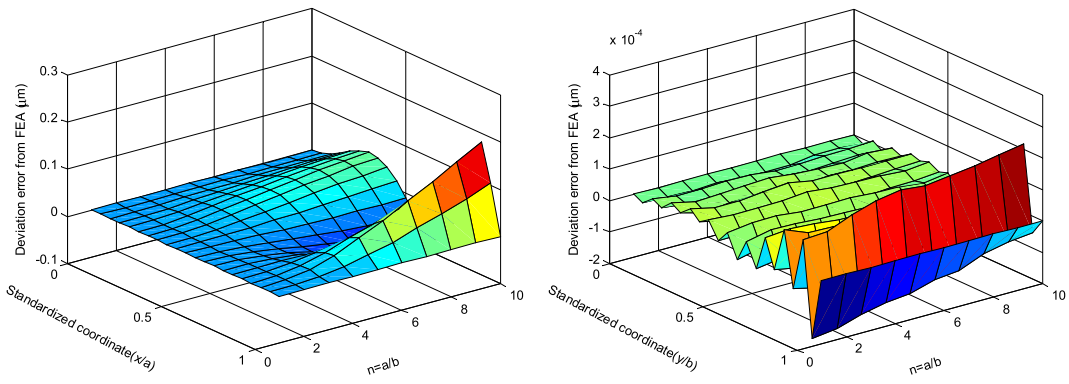

(a) x-axis (b) y-axis

Fig. 2. Deviation error from FEA results with n against standardized coordinate.

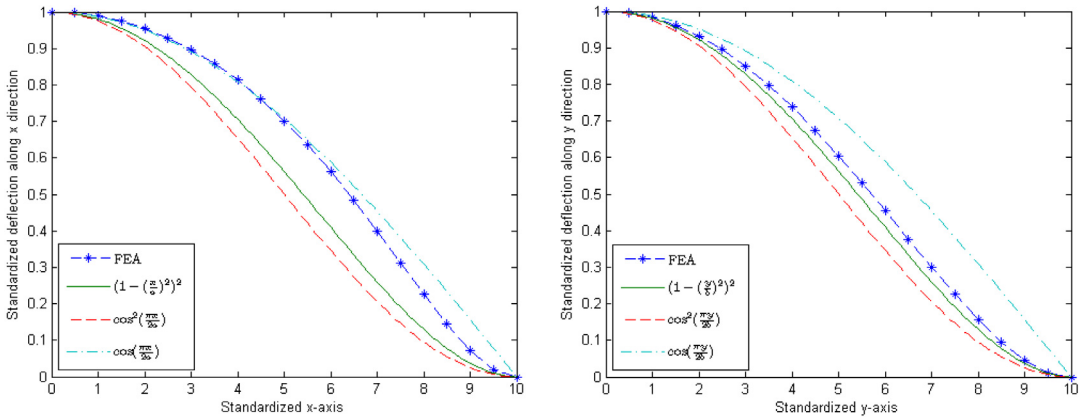

(a) x-axis (b) y-axis

Fig. 3. Comparison of FEA results with existing basic functions. $n = 1.5$, $a = 90$ μm, $b = 60$ μm, $h = 1$ μm, $U = 130$ V.

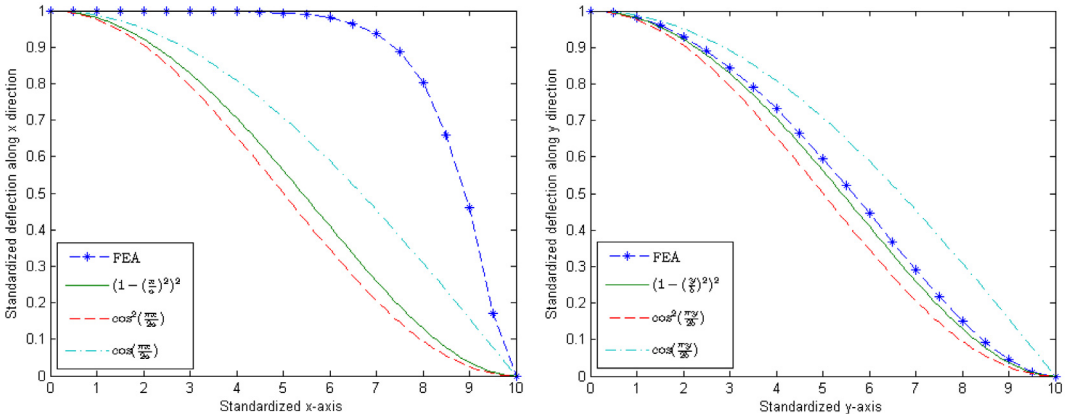

(a) x-axis (b) y-axis

Fig. 4. Comparison of FEA results with existing basic functions. $n = 6$, $a = 360$ μm, $b = 60$ μm, $h = 1$ μm, U = 120 V.

Table 3
The summed square of residuals between the basic functions and the FEA results. Membrane 1: $n = 1.5$, $a = 90$ μm, $b = 60$ μm, $h = 1$ μm, $U = 130$ V; membrane 2: $n = 6$, $a = 360$ μm, $b = 60$ μm, $h = 1$ μm, $U = 120$ V.

Membrane	Axis	S_1	S_2	S_3
Membrane 1	x-axis	0.18	0.37	0.04
	y-axis	0.02	0.09	0.19
Membrane 2	x-axis	3.43	4.06	1.70
	y-axis	0.01	0.08	0.21

After selecting the basic functions, the next step is establishing deflection shape function. Although function (6) is quite accurate when $1 \leqslant n < 4$, the parameters c_1, c_2, c_3 and c_4 have to be tuned every time the geometry dimension of the diaphragm changes. So the following analytical model is proposed to adjust to the changing geometry dimensions

$$\omega'_{1\leqslant n<4}(x,\ y) = \left(1-\frac{x^2}{a^2}\right)^2\left(1-\frac{y^2}{b^2}\right)^2\left(1+f_{l1}(n,\ h)\frac{x^2}{a^2}+f_{l2}(n,\ h)\frac{x^4}{a^4} + f_{s1}(n,\ h)\frac{y^2}{b^2}+f_{s2}(n,\ h)\frac{y^4}{b^4}\right), \tag{11}$$

where $f_{l1}(n,\ h)$, $f_{l2}(n,\ h)$, $f_{s1}(n,\ h)$ and $f_{s2}(n,\ h)$ are functions of n and h, which have a form as function (12).

$$\begin{aligned} f(n,\ h) = {} & (p_{34}n^4 + p_{33}n^3 + p_{32}n^2 + p_{31}n + p_{30})h^3 \\ & + (p_{24}n^4 + p_{23}n^3 + p_{22}n^2 + p_{21}n + p_{20})h^2 \\ & + (p_{14}n^4 + p_{13}n^3 + p_{12}n^2 + p_{11}n + p_{10})h \\ & + (p_{04}n^4 + p_{03}n^3 + p_{02}n^2 + p_{01}n + p_{00}) \end{aligned} \tag{12}$$

p_{rk}, $r = 0,\ 1,\ 2,\ 3$, $k = 0,\ 1,\ 2,\ 3,\ 4$, are corresponding coefficients. 30 and 70 sets of data are used to determine the coefficients of $f_{li}(n,\ h)$, $i = 1,\ 2$ and $f_{si}(n,\ h)$, $i = 1,\ 2$, respectively. For each set of data $f_{li}(n,\ h)$ and $f_{si}(n,\ h)$ are firstly calculated as constants using curve fitting tool in *MATLAB*. Subsequently, the constants are employed to determine the coefficients p_{ij} by surface fitting tool in *MATLAB*. The corresponding coefficients are given in Table 4.

When $n \geqslant 4$, basic function $R_4(x)$ is modified by combining with function $R_1(x)$ and adding two terms to improve the accuracy of predicting the deformed curve shape along x-axis, representing as

$$\omega'_{n\geqslant 4}(x,0) = \left(1-0.2^{f_{r0}(n,\ h)\cdot R_1(x)}\right)\left(1+f_{r1}(n,\ h)\cdot\frac{x^2}{a^2}+f_{r2}(n,\ h)\cdot\frac{x^4}{a^4}\right). \tag{13}$$

where $f_{rj}(n,\ h)$, $j = 0,\ 1,\ 2$ are functions of n and h, which also have a form as function (12). And the overall deflection shape function when $n \geqslant 4$ is proposed as follows:

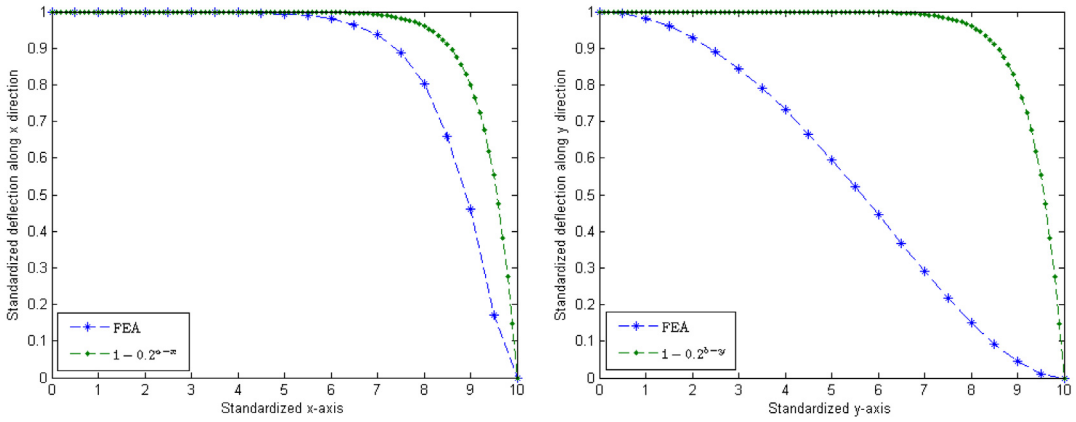

(a) x -axis (b) y -axis

Fig. 5. Comparison of FEA results with the new basic function. $n = 6,\ a = 360\ \mu m,\ b = 60\ \mu m,\ h = 1\ \mu m,\ U = 120\ V$.

Table 4
Coefficients of the corresponding functions used in the new deflection model.

Coefficients	f_{l1}	f_{l2}	f_{s1}	f_{s2}	f_{r0}	f_{r1}	f_{r2}
p_{34}	0.09553	0.476	7.75E−05	0.000252	0.1891	0.000484	−0.00991
p_{33}	−0.8566	−4.072	−0.00166	−0.0034	−4.91	−0.01175	0.2522
p_{32}	2.694	12.29	0.009036	0.002881	47.66	0.1131	−2.408
p_{31}	−3.372	−15.79	−0.02326	0.04715	−206.6	−0.4968	10.19
p_{30}	1.307	6.845	−0.1173	−0.3046	332.4	0.7895	−16.09
p_{24}	−0.2865	−1.465	−0.00043	−0.00092	−0.5873	−0.00164	0.02709
p_{23}	2.559	12.43	0.008716	0.01249	15.54	0.0389	−0.6938
p_{22}	−8.03	−37.21	−0.04498	−0.01105	−153.8	−0.361	6.685
p_{21}	9.958	47.88	0.09975	−0.17	681.4	1.524	−28.67
p_{20}	−3.634	−20.7	0.4992	1.132	−1122	−2.297	46.01
p_{14}	0.2796	1.397	0.000925	0.001179	0.565	0.002841	−0.02336
p_{13}	−2.517	−11.69	−0.0173	−0.01592	−15.62	−0.06608	0.6026
p_{12}	8.022	34.58	0.0841	0.0164	161.2	0.5783	−5.872
p_{11}	−10.01	−44.94	−0.1608	0.2053	−747.3	−2.226	25.63
p_{10}	3.341	19.43	−0.7785	−1.459	1286	2.954	−42.12
p_{04}	−0.06217	−0.4242	0.000618	−8.1E−05	−0.105	−0.00177	0.006645
p_{03}	0.5711	3.356	−0.01381	−0.00142	3.013	0.04372	−0.1691
p_{02}	−2.115	−8.817	0.1215	0.0466	−31.58	−0.4111	1.617
p_{01}	3.736	11.56	−0.4201	−0.2343	152.1	1.738	−6.802
p_{00}	−1.24	−5	1.18	0.8695	−255.1	−2.556	9.772

$$\omega'_{n\geqslant 4}(x,\ y) = \left(1 - 0.2^{f_{r0}(n,\ h)\cdot R_1(x)}\right)\left(1 - \frac{y^2}{b^2}\right)^2 \left(1 + f_{r1}(n,\ h)\cdot\frac{x^2}{a^2} + f_{r2}(n,\ h)\cdot\frac{x^4}{a^4} + f_{s1}(n,\ h)\frac{y^2}{b^2} + f_{s2}(n,\ h)\frac{y^4}{b^4}\right) \quad (14)$$

40 sets of data are used to determine functions $f_{rj}(n,\ h)$, and the corresponding coefficients are listed in Table 4.

Eqs. (11) and (14) can be combined by using a piecewise function to derive an analytical deflection shape function for rectangular membranes whenever $n \geqslant 1$ as

$$\omega'(x,\ y) = h(c-n)\cdot\omega'_{1\leqslant n<4}(x,\ y) + h(n-4)\cdot\omega'_{n\geqslant 4}(x,\ y),\ n \geqslant 1 \quad (15)$$

where the piecewise function is defined as $h(t) = \begin{cases} 0, & t < 0 \\ 1, & t \geqslant 0 \end{cases}$, and c is a positive constant infinitely approaching 4 but less than 4.

Subsequently, the analytical deflection model for rigidly clamped rectangular membranes can be achieved by multiplying ω_0 and $\omega'(x,\ y)$ as

$$\omega(x,\ y) = \omega_0\cdot\omega'(x,\ y). \quad (16)$$

4. Deflection model validation

The validity of analytical deflection model (16) can be verified in two aspects: similarity of deformed curves and error in capacitance values between model calculated results and FEA results. The gap thickness d_0 is given as 2 μm in all the tests. As a result, the maximum deflections of membranes are near 0.7 μm in the non-collapse mode. As small and large deflection are relative concept, deflections near 0.7 μm are considered as large deflections in this chapter, while deflections less than 20% of membrane thicknesses are treated as small deflections. Similarly, membrane thicknesses near 0.6 μm are seen as thin membranes and those near 1.5 μm are considered as thick ones. Different cases will be investigated in the following.

4.1. Similarity of deformed curves

Figs. 6 and 7 show comparisons of FEA-derived-deflection profiles with model-predicted deflection curves for small deflection case for diaphragms with $n = 1.5$ and $n = 5$, respectively. The deflection profiles are plotted from the diaphragms center along

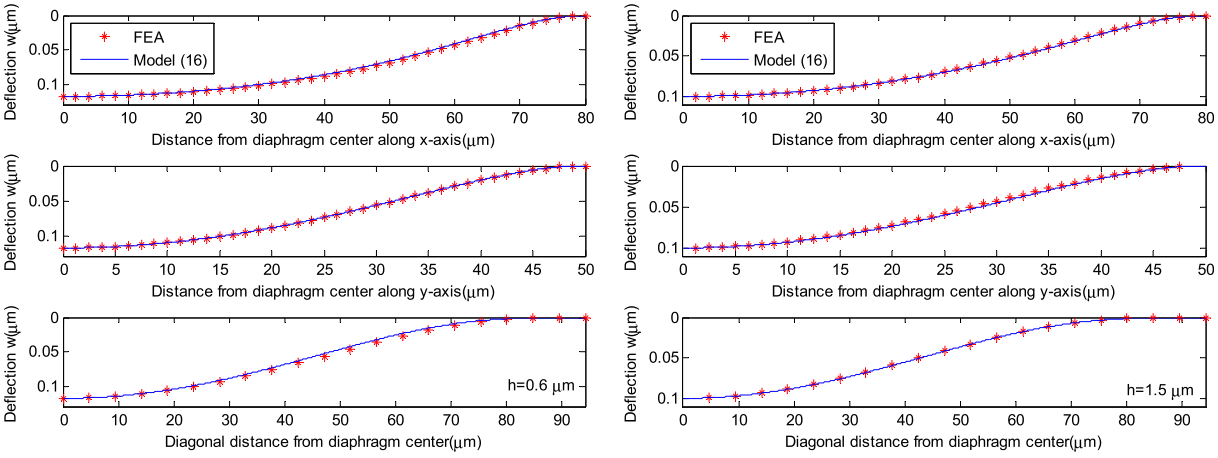

(a) $a = 80\mu m, b = 50\mu m, h = 0.6\mu m, U = 70V$ (b) $a = 80\mu m, b = 50\mu m, h = 1.5\mu m, U = 170V$

Fig. 6. Comparison of FEA deflection profiles with the new model for membranes with $n = 1.6$ for small deflection.

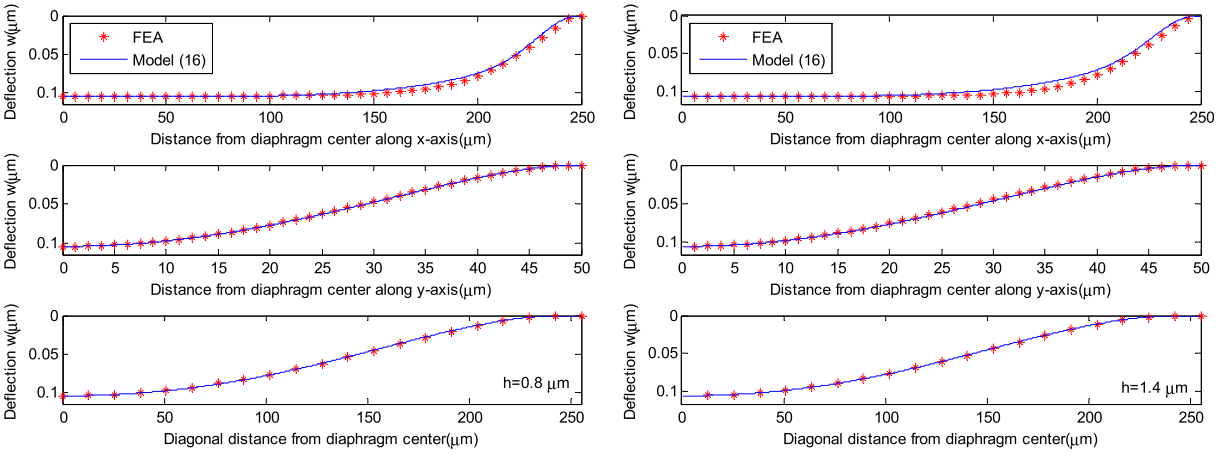

(a) $a = 250\mu m, b = 50\mu m, h = 0.8\mu m, U = 80V$ (b) $a = 250\mu m, b = 50\mu m, h = 1.4\mu m, U = 150V$

Fig. 7. Comparison of FEA deflection profiles with the new model for membranes with $n = 5$ for small deflection.

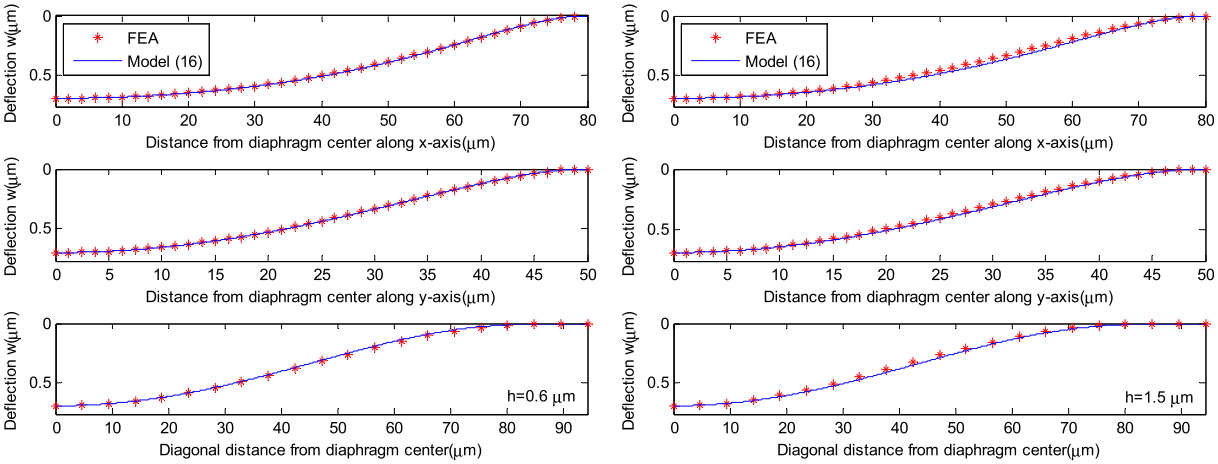

(a) $a = 80\mu m, b = 50\mu m, h = 0.6\mu m, U = 147V$ (b) $a = 80\mu m, b = 50\mu m, h = 1.5\mu m, U = 365V$

Fig. 8. Comparison of FEA deflection profiles with the new model for membranes with $n = 1.6$ for large deflection.

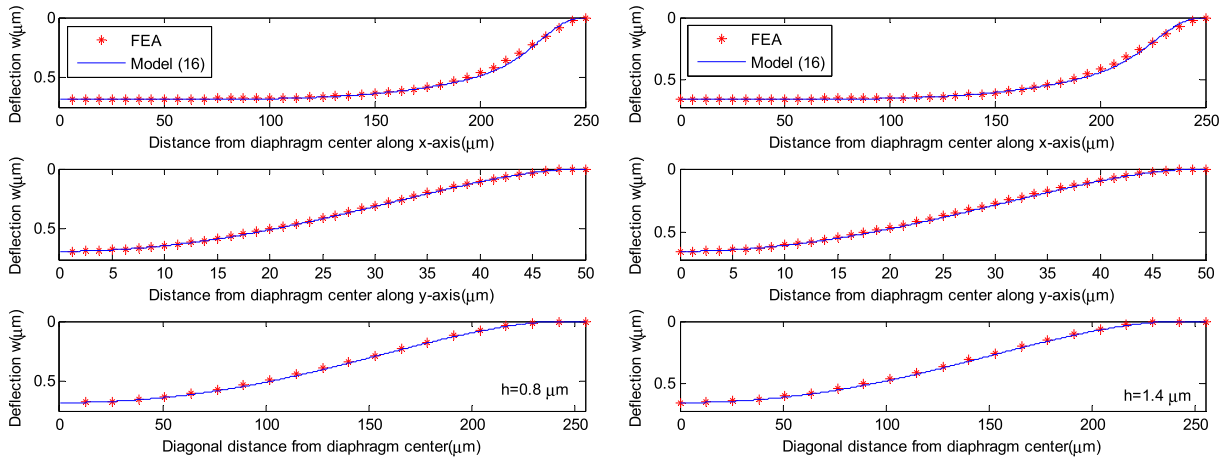

(a) $a = 250\mu m, b = 50\mu m, h = 0.8\mu m, U = 170V$ (b) $a = 250\mu m, b = 50\mu m, h = 1.4\mu m, U = 300V$

Fig. 9. Comparison of FEA deflection profiles with the new model for membranes with $n = 5$ for large deflection.

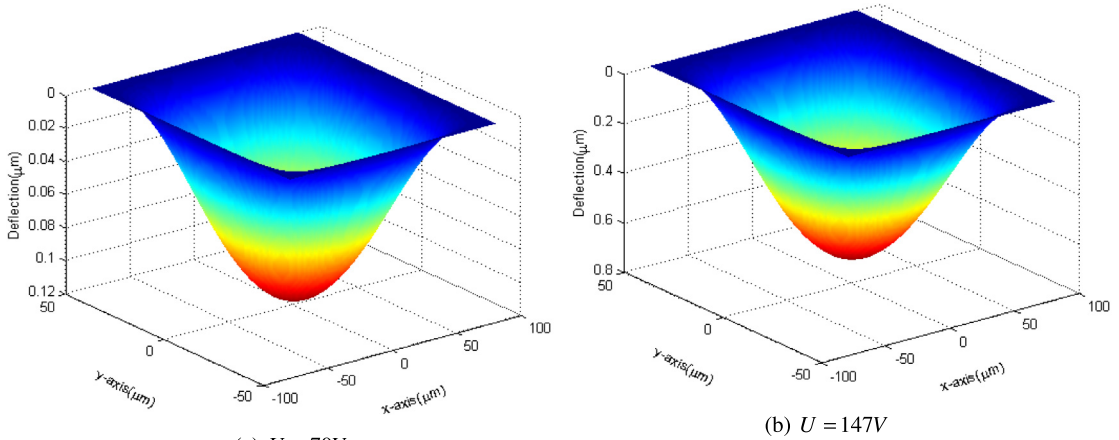

(a) $U = 70V$ (b) $U = 147V$

Fig. 10. Deflection profiles of a membrane under different DC bias voltages. $a = 80$ μm, $b = 50$ μm, $h = 0.6$ μm.

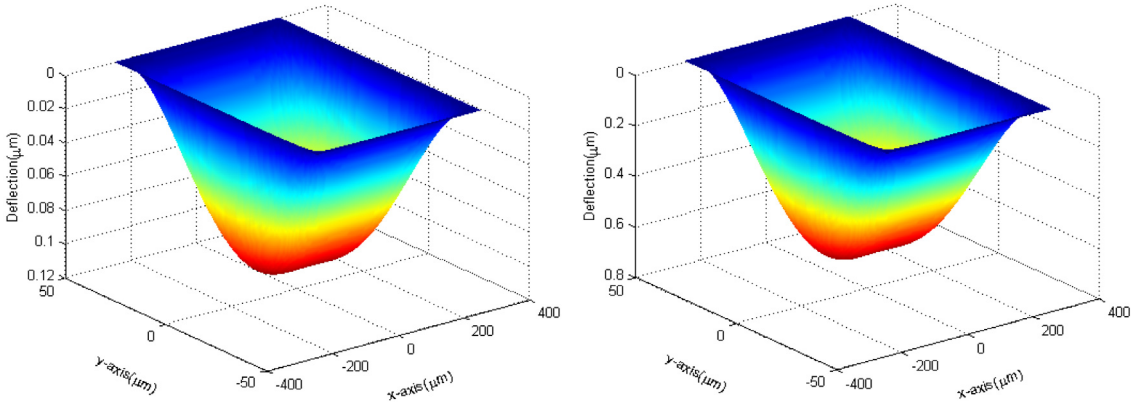

(a) $U = 150V$ (b) $U = 300V$

Fig. 11. Deflection profiles of a membrane under different DC bias voltages. $a = 250$ μm, $b = 50$ μm, $h = 1.4$ μm.

Table 5
Comparison of capacitance values between new model-calculated results and FEA results. $d_0 = 2$ μm for all cases.

Deflection	a (μm)	b (μm)	h (μm)	U (V)	ω_0 (μm)	Capacitance value (fF)		%ΔC |FEA − analytical|
						FEA	Model (16)	
Small	50	50	0.6	75	0.085	44.932	44.892	0.088
	50	50	1.5	200	0.079	44.828	44.818	0.023
	180	60	0.7	55	0.104	195.726	195.361	0.186
	180	60	1.3	100	0.103	195.435	195.225	0.107
	420	70	0.6	40	0.105	535.196	534.343	0.159
	420	70	1.5	85	0.088	531.944	531.267	0.127
	325	250	0.6	11	0.100	1471.392	1463.600	0.530
	325	250	1.5	20	0.114	1472.576	1466.000	0.265
Large	50	50	0.6	185	0.684	50.807	50.704	0.203
	50	50	1.5	485	0.702	50.342	50.600	0.512
	180	60	0.7	115	0.661	225.126	224.686	0.195
	180	60	1.3	205	0.671	223.296	224.573	0.572
	420	70	0.6	83	0.702	641.708	642.641	0.145
	420	70	1.5	185	0.703	631.776	633.984	0.349
	325	250	0.6	22	0.621	1670.552	1629.900	2.433
	325	250	1.5	38	0.645	1657.636	1628.800	1.740

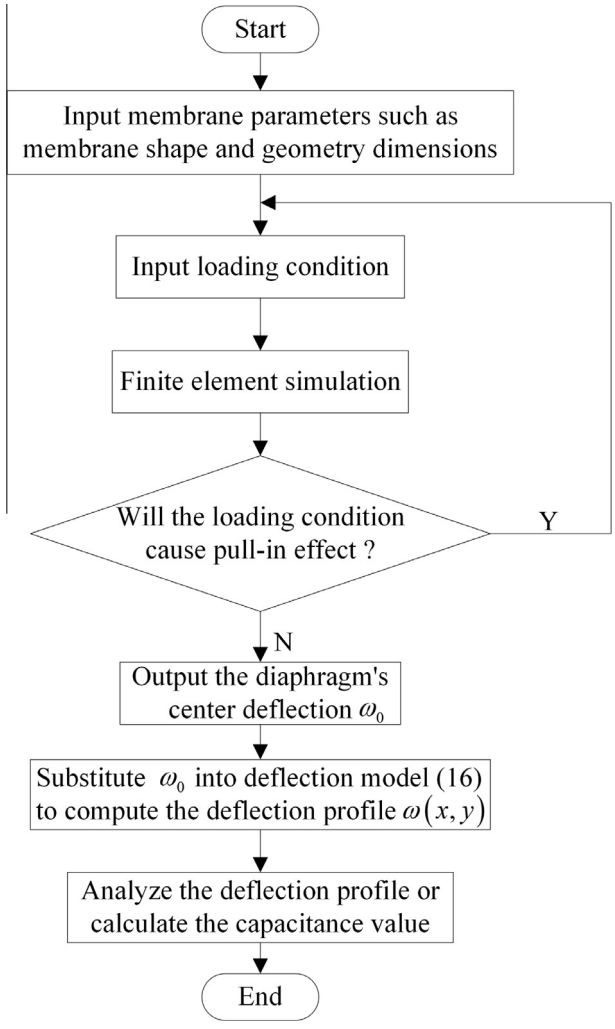

Fig. 12. Flowchart of how the new model is used in practice.

x-axis, y-axis and diagonal direction towards the top right corner of clamped diaphragms. Although a slight error appears along x-axis when $h = 1.4$ μm and $n = 5$, it is acceptable considering the error is extremely small. Overall, excellent agreement between the new analytical model and the FEA results can be observed for both thin and thick membranes.

The same diaphragms under relatively larger DC bias voltages are employed for comparisons for large deflection case, shown in Figs. 8 and 9. It can be observed that the model-predicted deflection profiles are still in excellent agreement with the corresponding FEA results for membranes with different thicknesses and aspect ratios. The figures clearly demonstrate that the new deflection model (16) is able to accurately describe the deformation of rectangular membranes under electrostatic pressure.

Now that the effectiveness of the new deflection model has been verified, it could be used to analyze the deflections of rectangular membranes. Figs. 10 and 11 show deflection profiles of two membranes under different DC bias voltages. From each figures, it can be seen that different loading conditions do not have much influence on the deflection shape of the membrane while they mainly affect the center deflection. And comparison between Figs. 10 and 11 shows that deflection shapes of membranes with different aspect ratios and thicknesses have significant difference. Specifically, Fig. 11 reveals that most of the deflection of the membrane with aspect ratio 5 occurs in the center, which makes the added length (the two ends) not that useful because it does not deflect by much. Therefore, such design of membrane could be improved by shortening the length or extending the width.

4.2. Error in capacitance values

The capacitance values of CMUTs can be calculated by combining deflection model (16) and formula (5). 50 groups of membranes of different kinds (thin and thick, diverse aspect ratios, large deflection and small deflection, different loading conditions) are employed to validate the new deflection model. Some of the typical comparisons between the model-calculated capacitance values and the FEA-derived results are listed in Table 5. And high accuracy of the model-calculated results can be observed from the table. To be more specific, the maximum deviation from the FEA results is 2.433% in the 50 groups of random tests.

5. Conclusions

A new deflection shape function that predicts the deflection profiles of CMUTs with rectangular membranes has been proposed. It is established to accurately describe the deformations of CMUT membranes with a wide range of geometry dimensions and

loading conditions. The predictions of membrane deflection profiles show excellent agreements with FEA results. Fig. 12 is a flowchart that shows how the new deflection model is used in practice. First of all, the membrane parameters such as material properties, geometry dimensions and loading conditions are used to calculate the diaphragm's center deflection ω_0 by FEM. The load on the membrane will be reduced if it causes pull-in effect. Then the center deflection ω_0 is substituted into model (16) to compute the deflection profile $\omega(x, y)$. Subsequently, the capacitance between the deformed membrane and the fixed back plate is calculated using Eq. (5). The highly accurate deflection shape function we have developed provides a simple and easy method for designers to analyze the effects of the design parameters such as geometry dimensions on the performance of CMUTs.

Conflict of interest

The authors declare that there are no conflict of interest.

Acknowledgements

This work is supported by National Basic Research Program of China (973 program) under Grant 2014CB845302 and by National Natural Science Foundation (NNSF) of China under Grants 61374036, 61273121, and Natural Science Foundation of Guangdong Province under Grant 2014A030313237, and by Natural Science and Engineering Research Council of Canada.

References

[1] O. Oralkan, A.S. Ergun, J.A. Johnson, M. Karaman, U. Demirci, K. Kaviani, T.H. Lee, B.T. Khuri-Yakub, Capacitive micromachined ultrasonic transducers: next-generation arrays for acoustic imaging?, IEEE Trans Ultrason. Ferroelectr. Freq. Control 49 (11) (2002) 1596–1610.
[2] A. Logan, J.T.W. Yeow, Fabricating capacitive micromachined ultrasonic transducers with a novel silicon-nitride-based wafer bonding process, IEEE Trans. Ultrason. Ferroelectr. Freq. Control 56 (5) (2009) 1074–1084.
[3] R. Puers, D. Lapadatu, Electrostatic forces and their effects on capacitive mechanical sensors, Sens. Actuators A Phys. 56 (3) (1996) 203–210.
[4] Y. Huang, E.O. Haeggstrom, X. Zhuang, A.S. Ergun, B.T. Khuri-Yakub, Optimized membrane configuration improves CMUT performance, in: Proc. IEEE Ultrason. Symp., 2004, pp. 505–508.
[5] S. Zhou, P. Reynolds, J.A. Hossack, Improving the performance of capacitive micromachined ultrasound transducers using modified membrane and support structures, in: Proc. IEEE Ultrason. Symp, 2005, pp. 1925–1928.
[6] O. Onen, R. Guldiken, Detailed investigation of capacitive micromachined ultrasonic transducer design space, Microsyst. Technol. 18 (4) (2012) 399–408.
[7] P.-C. Eccardt, P. Wagner, S. Hansen, Analytical models for micromachined transducers-an overview, in: Proc. IEEE Ultrason. Symp., 2006, pp. 572–581.
[8] I.O. Wygant, M. Kupnik, B.T. Khuri-Yakub, Analytically calculating membrane displacement and the equivalent circuit model of a circular CMUT cell, in: Proc. IEEE Ultrason. Symp., 2008, pp. 2111–2114.
[9] A. Lohfink, P.-C. Eccardt, Linear and nonlinear equivalent circuit modeling of CMUTs, IEEE Trans. Ultrason. Ferroelectr. Freq. Control 52 (12) (2005) 2163–2172.
[10] S.A. Anbalagan, G. Uma, M. Umapathy, Modeling and simulation of capacitive micromachined ultrasonic transducer (CMUT), J. Phys.: Conf. Ser. 34 (2006) 595–600.
[11] H. Köymen, M.N. Senlik, A. Atalar, S. Olcum, Parametric linear modeling of circular CMUT membranes in Vacuum, IEEE Trans. Ultrason. Ferroelectr. Freq. Control 54 (6) (2007) 2163–2172.
[12] S. Timoshenko, S. Woinosky-Krieger, Theory of Plates and Shells, McGraw Hill Classic Textbook Reissue, second ed., 1959.
[13] D. Maier-Schneider, J. Maibach, E. Obermeier, A new analytical solution for the load-deflection of square membranes, J. Microelectromech. Syst. 4 (4) (1995) 238–241.
[14] M. Rahman, S. Chowdhury, A new deflection shape function for square membrane CMUT design, in: Proc. IEEE Int. Symp. Circuits Syst., 2010, pp. 2019–2022.
[15] M. Rahman, S. Chowdhury, Square diaphragm CMUT capacitance calculation using a new deflection shape function, J. Sens. (2011) 1–12.
[16] S.D. Senturia, Microsystem Design, Kluwer Academic, Boston, 2001.
[17] A. Lohfink, P.-C. Eccardt, W. Benecke, H. Meixner, Derivation of a 1D CMUT model from FEM results for linear and nonlinear equivalent circuit simulation, in: Proc. IEEE Ultrason. Symp, 2003, pp. 465–468.
[18] B. Bayram, G.G. Yaralioglu, M. Kupnik, A.S. Ergun, Ö. Oralkan, A. Nikoozadeh, B.T. Khuri-Yakub, Dynamic analysis of capacitive micromachined ultrasonic transducers, IEEE Trans. Ultrason. Ferroelectr. Freq. Control 52 (12) (2005) 2270–2275.
[19] G.G. Yaralioglu, S.A. Ergun, B.T. Khuri-Yakub, Finite-element analysis of capacitive micromachined ultrasonic transducers, IEEE Trans. Ultrason. Ferroelectr. Freq. Control 52 (12) (2005) 2185–2198.
[20] G.G. Yaralioglu, B. Bayram, A. Nikoozadeh, B.T. Khuri-Yakub, Finite element modeling of capacitive micromachined ultrasonic transducers, in: Proc. SPIE, 2005, pp. 77–86.
[21] Y. Qian, N.R. Harris, P. Glynne-Jones, S.P. Beeby, A new 2-D model of a thin annular disk using a modified assumption, IEEE Trans. Ultrason. Ferroelectr. Freq. Control 57 (2) (2010) 421–426.
[22] Y. Huang, E.O. Haeggstrom, X. Zhuang, A.S. Ergun, B.T. Khuri-Yakub, Optimized membrane configuration improves CMUT performance, in: Proc. IEEE Ultrasonics Symp., 2004, pp. 505–508.
[23] Y. Huang, X. Zhuang, E.O. Haeggstrom, A.S. Ergun, C.-H. Cheng, B.T. Khuri-Yuaub, Capacitive micromachined ultrasonic transducers with piston-shaped membranes: fabrication and experimental characterization, IEEE Trans. Ultrason. Ferroelectr. Freq. Control 56 (1) (2009) 136–145.